remote sensing

MDPI

Article

Holocene Activity of the Wudaoliang–Changshagongma Fault of the Eastern Tibetan Plateau

Mingjian Liang [1,2,*], Yun Dong [3], Cheng Liao [1,2], Yulong Qin [4], Huiping Zhang [5], Weiwei Wu [1,2], Hong Zuo [1,2], Wenying Zhou [1,2], Changli Xiong [4], Li Yang [1,2], Yue Gong [1] and Tian Li [1]

[1] Sichuan Earthquake Agency, Chengdu 610041, China
[2] Chengdu Institute of Tibetan Plateau Earthquake Research, China Earthquake Administration, Chengdu 610041, China
[3] Nuclear Industry Southwest Geotechnical Investigation & Design Institute Co., Ltd., Chengdu 610051, China
[4] Sichuan Geological Survey Institute, Chengdu 610081, China
[5] State Key Laboratory of Earthquake Dynamics, Institute of Geology, China Earthquake Administration, Beijing 100029, China
* Correspondence: liangmingjian@scdzj.gov.cn

Abstract: The Wudaoliang–Changshagongma fault is one of the NW-trending faults located within the southern Bayan Har Block of the Tibetan Plateau in China. In this paper, we used high-resolution imagery and digital elevation model data to study the geomorphological and geological characteristics of the fault. Furthermore, the result also determined the fault trace and estimated the average horizontal slip rate of the fault since the late Quaternary to have been 2.6 ± 0.6 mm/a. This slip rate is approximately equivalent to that of the Awancang, Madoi–Garde, and Dari faults, which are also located within the block. Furthermore, the slip rates of these faults obtained by remote sensing and geological methods are consistent with GPS observations. It indicates that tectonic deformation within the block is continuous and diffuse. Using trenching study results and sedimentary radiocarbon dating, we identified four paleoearthquake events that occurred at 42,378–32,975, 33,935–20,663, 5052–4862, and after 673–628 cal BP, respectively. The recurrence intervals of large earthquakes on the faults within the block are much longer than those of the boundary faults, and the slip rates are also smaller, indicating that faults within the block play a regulatory role in the tectonic deformation of the Bayan Har Block.

Keywords: Wudaoliang–Changshagongma fault; fault slip rate; Bayan Har Block; geomorphological and geological characteristics

Citation: Liang, M.; Dong, Y.; Liao, C.; Qin, Y.; Zhang, H.; Wu, W.; Zuo, H.; Zhou, W.; Xiong, C.; Yang, L.; et al. Holocene Activity of the Wudaoliang–Changshagongma Fault of the Eastern Tibetan Plateau. *Remote Sens.* **2023**, *15*, 2458. https://doi.org/10.3390/rs15092458

Academic Editor: Yanxiu Shao

Received: 17 March 2023
Revised: 29 April 2023
Accepted: 30 April 2023
Published: 7 May 2023

1. Introduction

On 22 May 2021, the Madoi M7.4 earthquake occurred on the Jiangcuo fault inside the Bayan Har Block, China [1,2], which is one of the blocks of the Tibetan Plateau that has been most active during the Cenozoic [3–7]. Previously, on 17 March 1947, the Dari M7.7 earthquake occurred on the Dari fault within the block [8,9]. These seismic events indicate that faults within the block also experienced late Quaternary activity and had tectonic conditions capable of producing strong earthquakes. The Awancang (AWC), Madoi–Garde (MG), Dari (DR), and Wudaoliang–Changshagongma (WC) faults are the main strike-slip faults within the Bayan Har Block, China (Figure 1) [8–11]; however, their late Quaternary activity has been rarely studied in comparison with that of the boundary faults of the block, which are located on the north and south sides of the interior ones. The WC fault is a large strike-slip fault within the Bayan Har Block that is located to the north of the Garzê–Yushu fault. Zhang et al. [12] first studied the WC fault and believed that only part of the western segment of the fault showed Holocene activity. Deng et al. [13] suggested that the fault had been active in the Quaternary, but they could not determine its level of activity since the late Pleistocene. On the basis of the database of the Seismotectonic Map

of China, Xu et al. [14] suggested that the fault had experienced no new activity since the late Quaternary. Following remote sensing interpretation, Wu et al. [15] suggested that the fault is a left-lateral strike-slip fault with moderate activity by remote sensing analysis. Obviously, there is a lack of consensus regarding the level of late Quaternary activity of the WC fault.

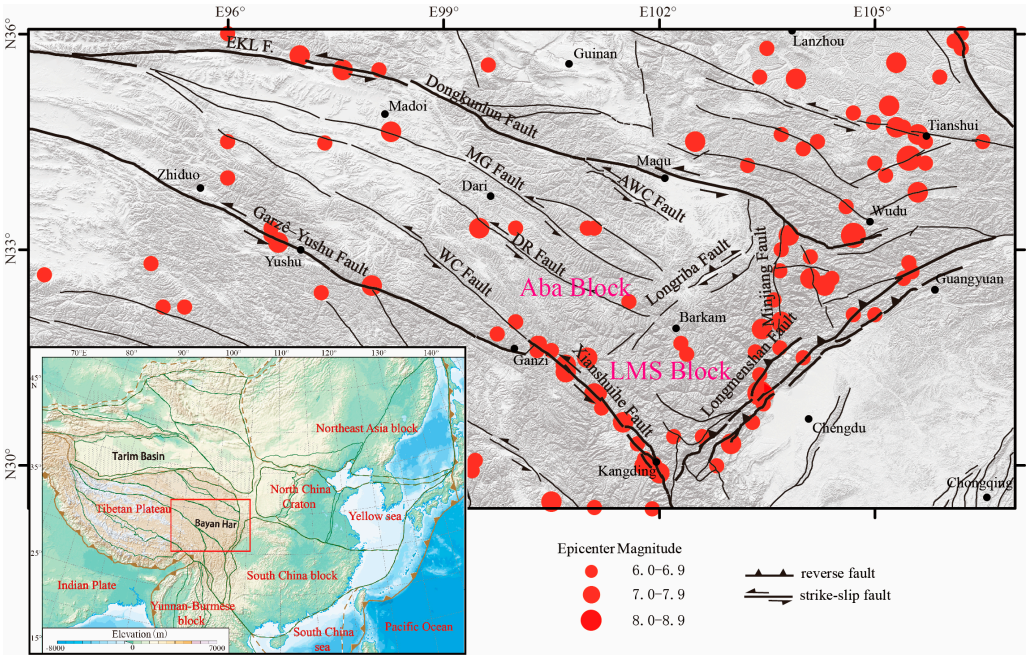

Figure 1. Map showing the main fault framework and seismicity characteristics of the Bayan Har Block. The Block can be subdivided into the Aba and Longmenshan subblocks by the Longriba fault.

The fault slip rate and a major earthquake sequence are important parameters in understanding fault activity and behavior. High-resolution remote sensing imagery and topographic data are essential elements for fine depiction of tectonic geomorphology, and many major discoveries in the field of active fault research have been made using such data [16–18]. For example, these data can be used to determine gully displacement along active faults, and identify the major earthquake behavior of faults by analyzing the distributional characteristics of gully offsets [15,17–21]. Moreover, LiDAR data of pre-earthquake and post-earthquake topography can be used to track the surface rupture of an earthquake, and obtain coseismic offset variables and other distributional characteristics [22–24].

In this study, we mapped the track of the middle segment of the WC fault using high-resolution satellite imagery, and obtained measurements of the left-lateral displacement of well-defined offset stream channels along the fault determined from unmanned aerial vehicle photogrammetry [25,26]. Then, we estimated the slip rate by sampling and dating the displaced landforms, and we obtained the paleoseismic sequence to establish the potential seismic hazard of the fault.

2. Tectonic Setting

The Bayan Har Block is one of the blocks of the Tibetan Plateau that has been most active during the Cenozoic [1–5]. The block experienced tectonic deformation associated with the Indosinian, Yanshanian, and Himalayan movements, and consists of widely distributed low-grade metamorphic Triassic sandstone [27–30]. The tectonic framework of the block was formed during the Yanshanian period, and its tectonic deformation was characterized by differential and intermittent uplift in the Himalayan periods [31,32].

The Bayan Har Block can be divided into the Aba and Longmenshan subblocks by the Longriba fault (Figure 1) [33–36]. As shown in Figure 1, earthquakes of ≥M7 have mainly occurred on the boundary faults of the block. However, the AWC, MG, DR, and WC faults

in the Aba subblock have late Quaternary activity and structural conditions conducive to the occurrence of major earthquakes [8–11]. The AWC fault is a left-lateral strike-slip fault with a slip rate in the Holocene of 3 mm/a [11]. The MG fault is also a Holocene active fault and its Holocene horizontal slip rate has been estimated as approximately 3 mm/a [10]. The DR fault, which is located in the middle of the block, and is also a Holocene fault. The horizontal slip rate of the DR fault was 2.6 mm/a, the surface rupture was approximately 70 km produced by the 1947 Dari M7.7 earthquake and it remains well preserved in its middle segment [9,37]. Although the WC fault has Holocene activity [37], reliable determination of the fault parameters has not been realized because of scant research. However, the 2022 Madoi M7.4 earthquake and the 1947 Dari M7.7 earthquake occurred on the Jiangcuo fault and the DR fault within the block, respectively, suggesting obvious deformation within the block and tectonic conditions suitable for the occurrence of large earthquakes.

3. Data and Methodology

To determine the late Quaternary active fault trace of the WC fault, we first used high-resolution satellite images from Google Earth and 12.5-m-resolution Shuttle Radar Topography Mission data to interpret the fault trace. The fault trace was interpreted based on geomorphic markers such as displaced gullies, linear fault scarps, and fault troughs. Subsequently, we conducted fieldwork along the fault and validated the interpretation of the fault trace. Unmanned aerial vehicle (UAV) and Structure from Motion (SfM) technology represent effective methods for quickly obtaining high-resolution digital orthographic images and digital elevation data of landforms [17,37–39]. Furthermore, we used these data sets for fine mapping of the fault trace, and to measure subtle geomorphic displacement and characterize fault behavior. On the basis of geological fieldwork, we selected typical dislocated landforms along the WC fault, such as dislocated gullies and alluvial fans, and obtained orthographic images and digital elevation model data of these landforms using the UAV and SfM technology to measure geomorphic offsets. Finally, we used these data and LaDiCaoz_V2 software to extract the displacement of dislocated landforms such as alluvial fans and gullies [17,24]. LaDiCaoz is a professional software developed by Zielke et al. [24] based on MATLAB for analyzing displacement of the strike-slip fault. This software can identify the optimal horizontal displacement value of a gully according to the user's input of fault location and upstream and downstream sections. The reliability of the estimated gully displacement can be verified by reconstructing the original landform prior to its displacement [17]. Additionally, we collected ^{14}C samples (organic sediment) of the displaced landforms, determined the times of the accumulated displacement of the landforms, and then calculated the average slip rate of the WC fault.

According to analysis of the geomorphology and sedimentary environment using high-resolution images, we selected sites suitable for trench excavation for paleoearthquake research on the WC fault. Furthermore, we analyzed the relationship between the deformation of strata and the faults revealed in the trench to identify the paleoearthquake sequence. We also identified the time of occurrence of the earthquakes based on the radiocarbon dating ages of the strata, and evaluated the major earthquake risk on the WC fault. The samples were tested at the Beta Analytic Inc. testing laboratory (Miami, FL, USA).

4. Results

4.1. Fault Activity and Slip Rate

The linear track of the WC fault is especially obvious in Changshagongma Town, in the north of Shiqu County (Sichuan Province, China). The fault controls the northern boundary of the Changshagongma Cenozoic basin (Figure 2). A series of gullies and alluvial–proluvial fans along the fault have left-lateral displacement, forming tectonic landforms such as fault troughs, scarps, and sag ponds.

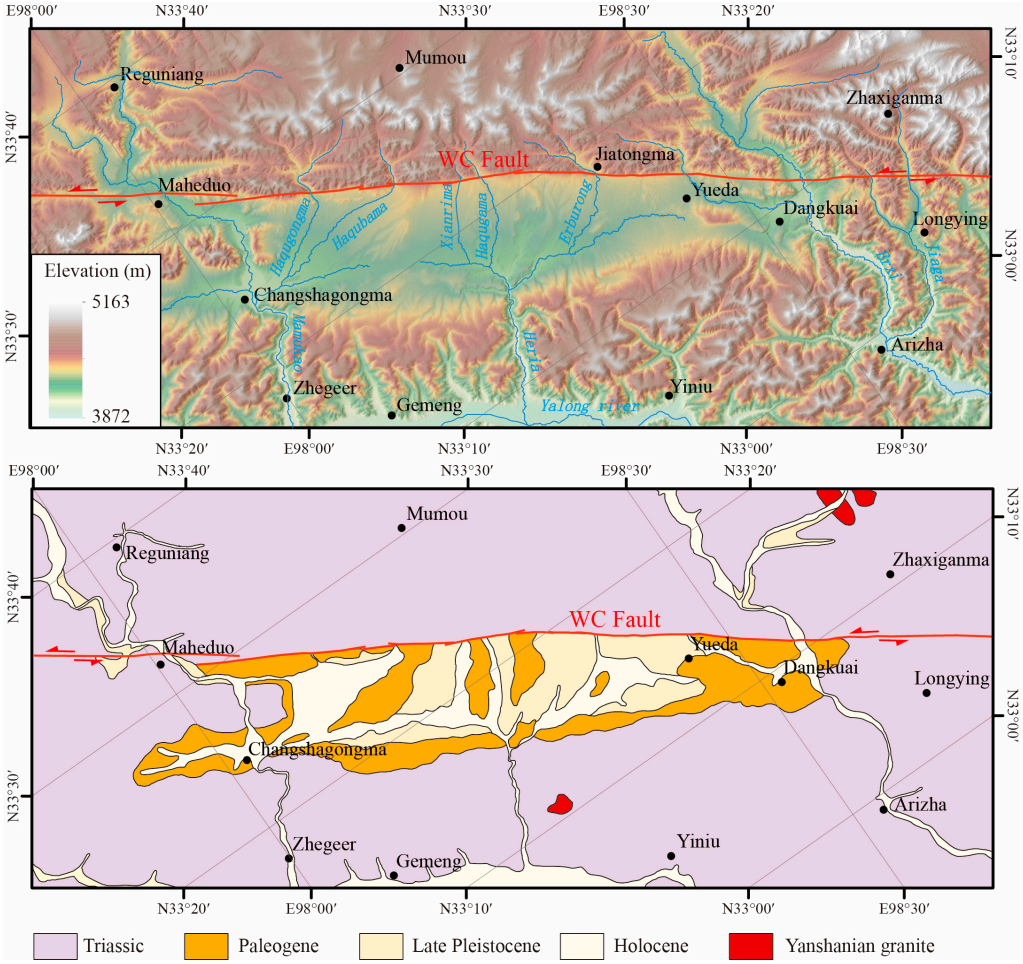

Figure 2. Geological and geomorphological maps along the middle segment of the WC fault. Black squares represent the locations of fieldwork sites. The WGS 1984 Datum is used for the geographic coordinate in the figure.

On the west side of the mouth of the Haqugongma River, the WC fault cuts through the hillside, forming a fault trough and developing fault springs (Figure 3A). To the east of the river mouth, the fault cuts through a piedmont alluvial fan, leading to a series of gully displacement and forming a linear fault scarp (Figure 3B). We used the UAV and ESRI ArcMap to obtain digital images of the landform (Figure 4A), and determined left-lateral displacement of approximately 20.0 m of a gully using LaDiCaoz_V2 (Figure 4C,D). We dug a pit on the alluvial fan to collect radiocarbon dating samples (the white triangle in Figure 4C identifies the sampling position). The excavated profile of the pit revealed two sets of strata (Figure 4B): unit ①, a reddish-brown sandy soil layer containing abundant plant debris, gravels, and organic matter; and unit ②, a sandy gravel layer formed by alluvial deposition. The conventional radiocarbon age of sample WC2022-1, collected near the top of unit ②, is 7615–7486 cal BP (Figure 4B; Table 1). Therefore, we calculated the horizontal slip rate of the fault to be 2.6 mm/a at this site. Another gully in the northeastern corner of Figure 4C has no obvious displacement (Figure 4C), probably because it was eroded and not preserved.

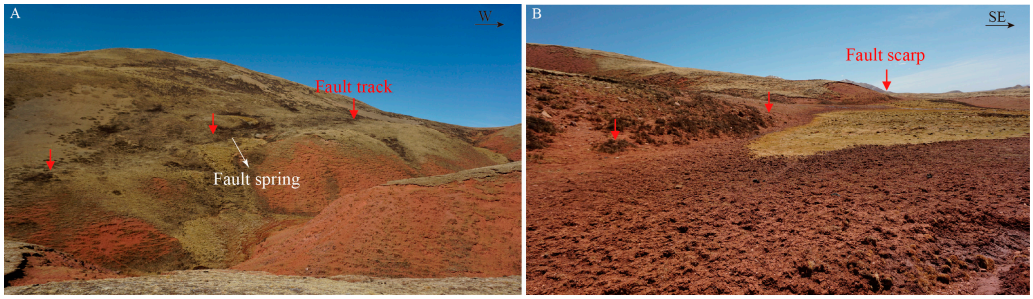

Figure 3. Fault trace and tectonic landforms of the WC fault on the west side of the mouth of the Haqugongma River: (**A**) a fault trough and spring along the fault; and (**B**) a linear fault scarp. Red arrows mark the fault traces.

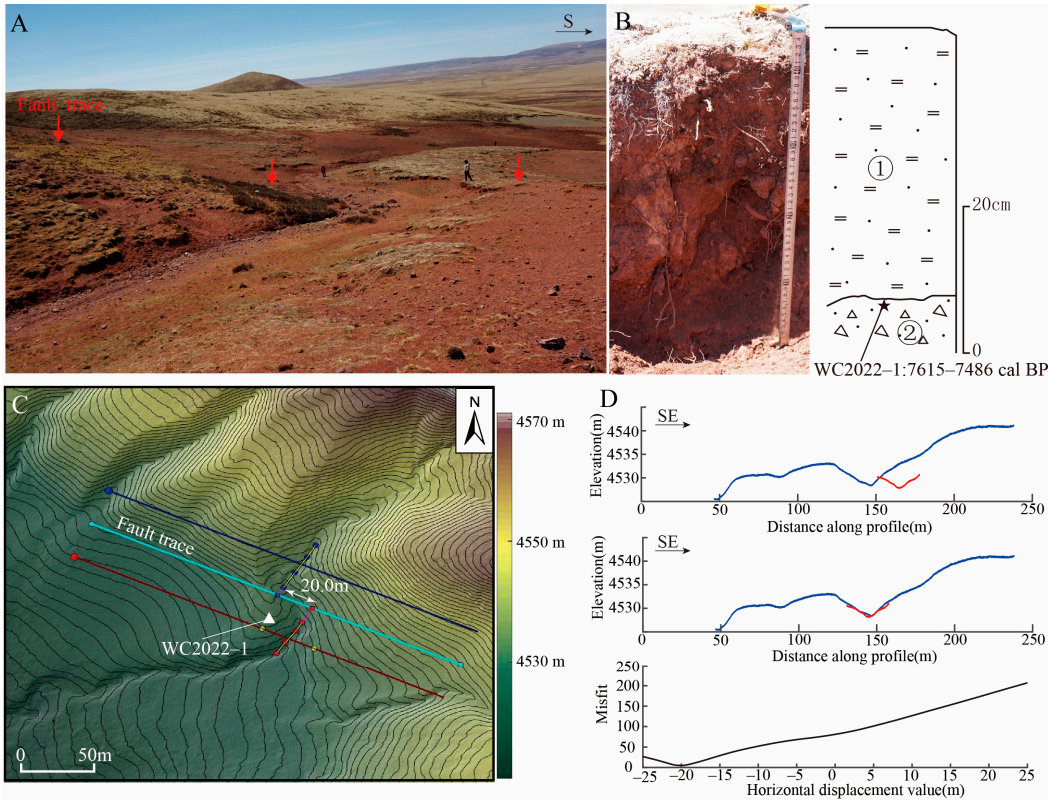

Figure 4. (**A**) Left-lateral displacement (approximately 20.0 m) of a gully on the west side of the mouth of the Haqugongma River, identified using UAV photogrammetry and LaDiCaoz_V2. (**B**) Geological section and radiocarbon sample obtained from position identified by the white triangle in (**C**). (**C**,**D**) Displacement of the gully as determined using LaDiCaoz_V2. Red arrows mark the fault traces. The blue and red lines represent the gully profiles on both sides of the fault in Figure 4D, respectively.

The WC fault extends in the SE direction and cuts through the Holocene diluvial fans in the piedmont. This fault segment consists of multiple branches in a right-stepping echelon, forming an extrusion bulge, linear reverse scarps, and sag ponds on the diluvial fan formed in the Holocene (Figure 5).

To the west of the mouth of the Xierimagou River, the WC fault has formed multi-branched fault scarps on the diluvial fan in front of the mountain (Figure 6A). The main fault scarp, which is aligned in the NW–SE direction, has a height of approximately 2–3 m (Figure 6B). In front of the main scarp, there are multiple secondary scarps with a height of approximately 0.2–0.5 m (Figure 6C), which might have been produced by the latest major earthquake on the fault.

Table 1. Test results of the radiocarbon samples of this study.

Sample Number	Longitude (°)	Latitude (°)	Lab. Number	Sample Material	13C/12C (o/oo)	Measured Radiocarbon Age (a BP)	Conventional Radiocarbon Age (cal BP)
WC2022-1	98.14678	33.44694	642816	Organic sediment	−23.6	6670 ± 30	7615–7486
WC2022C-1	98.39852	33.29580	642820	Organic sediment	−23.0	2980 ± 30	3265–3106
WCTC-C14-01	98.30482	33.36158	607291	Organic sediment	−20.4	12,430 ± 40	15,052–14,782
WCTC-C14-04	98.30482	33.36158	612632	Organic sediment	−23.2	4370 ± 30	5052–4862
WCTC-C14-06	98.30482	33.36158	607292	Organic sediment	−23.4	3830 ± 30	4409–4225
WCTC-C14-08	98.30482	33.36158	612633	Organic sediment	−22.6	830 ± 30	800–688
WCTC-C14-12	98.30482	33.36158	607293	Organic sediment	−24.9	670 ± 30	673–628
WCTC-02	98.31697	33.35455	607294	Organic sediment	−23.6	37,480 ± 340	42,378–41,631
WCTC-05	98.31697	33.35455	612634	Organic sediment	−23.9	28,900 ± 140	33,935–32,975
WCTC-06	98.31697	33.35455	642812	Organic sediment	−23.1	38,820 ± 480	43,007–42,203
WCTC-11	98.31676	33.35509	642814	Organic sediment	−22.9	16,830 ± 50	20,517–20,258
WCTC-12	98.31676	33.35509	642815	Organic sediment	−22.9	17,250 ± 50	20,979–20,663
WCTC-14	98.31676	33.35509	607295	Organic sediment	−24.0	2520 ± 30	2598–2496

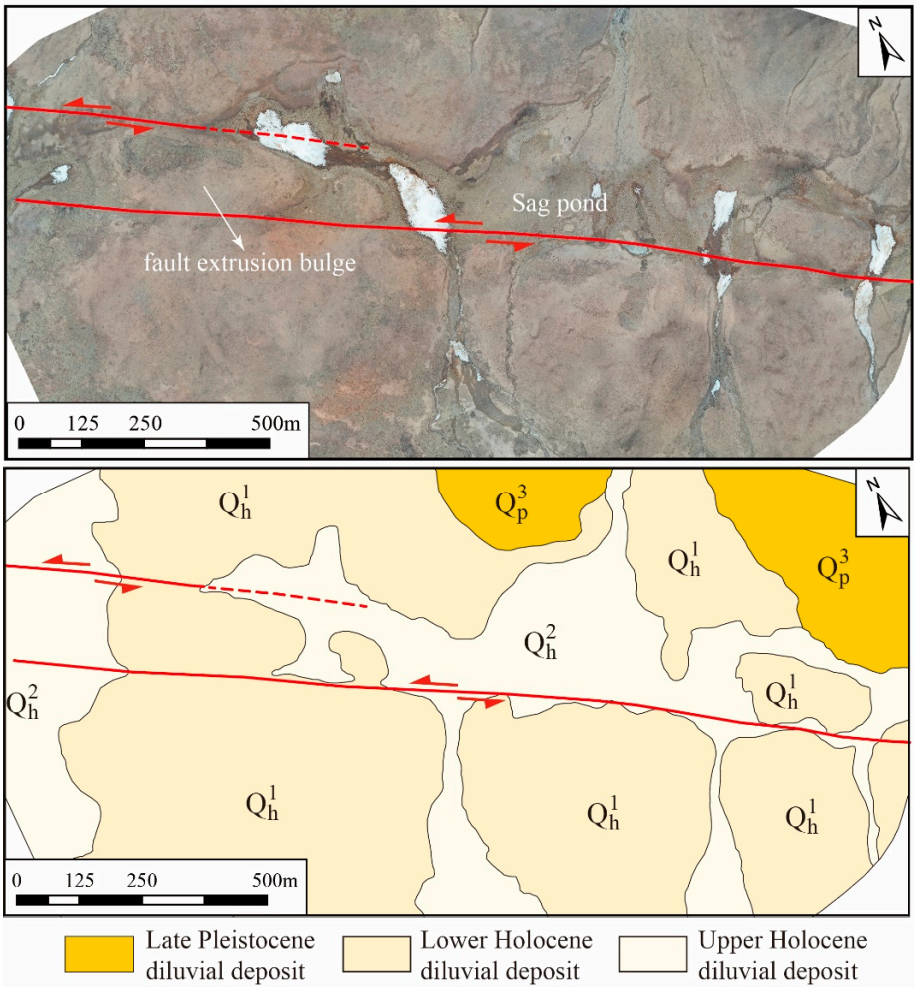

Figure 5. Fault trace and geomorphological characteristics on the west side of the mouth of the Haqugongma River. The image was obtained using UAV photogrammetry. The red dotted line shows the inferred fault trace.

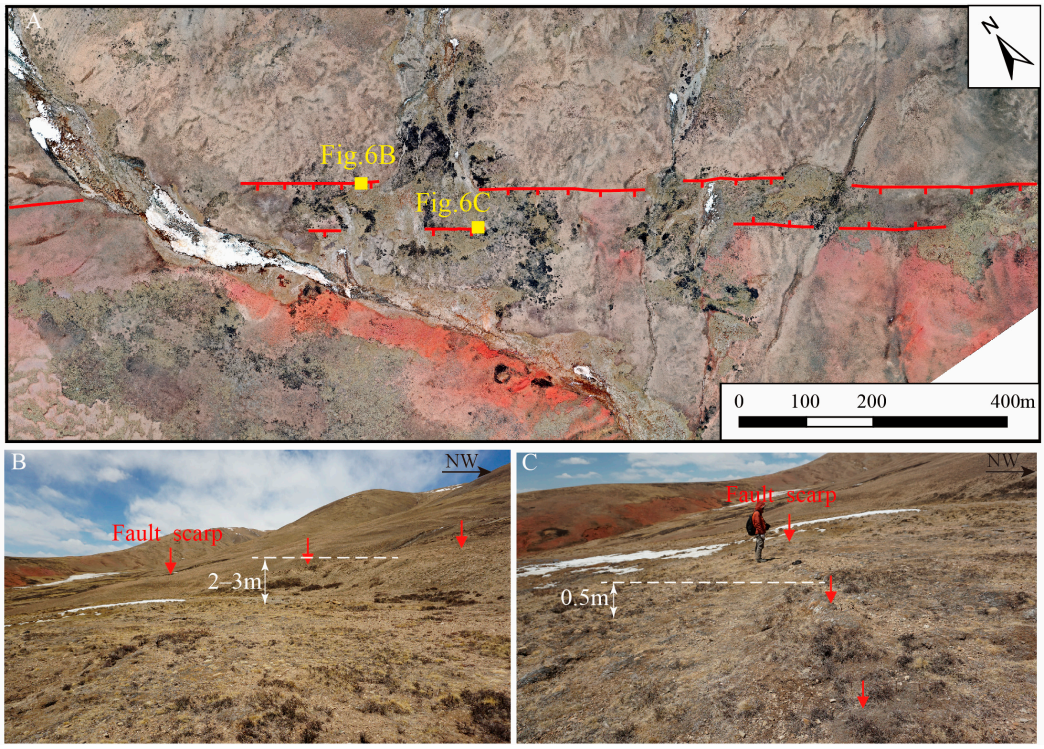

Figure 6. (**A**) Fault trace and geomorphological characteristics near the west of the mouth of the Xierimagou River. The image was obtained using UAV photogrammetry. (**B**) Fault scarp with height of 2–3 m (at position Figure 6B, shown in (**A**)). (**C**) An approximately 0.5 m-high fault scarp (at position Figure 6C shown in (**A**)). Red arrows mark the fault traces.

To the east of the mouth of the Haqugama River, the fault cut through the late Quaternary diluvial fan and produced a linear scarp and trough (Figure 7A). The fault left-laterally dislocated the diluvial fan by approximately 29.1 ± 2.4 m (Figure 7B). We excavated a trench on the diluvial fan across the linear fault scarp. According to the strata revealed in trench TC1 and the ^{14}C dating results (sample WCTC-C14-01), the age of the alluvial fan is 15,052–14,782 cal BP. Therefore, we determined a horizontal slip rate of 2.0 mm/a at this site.

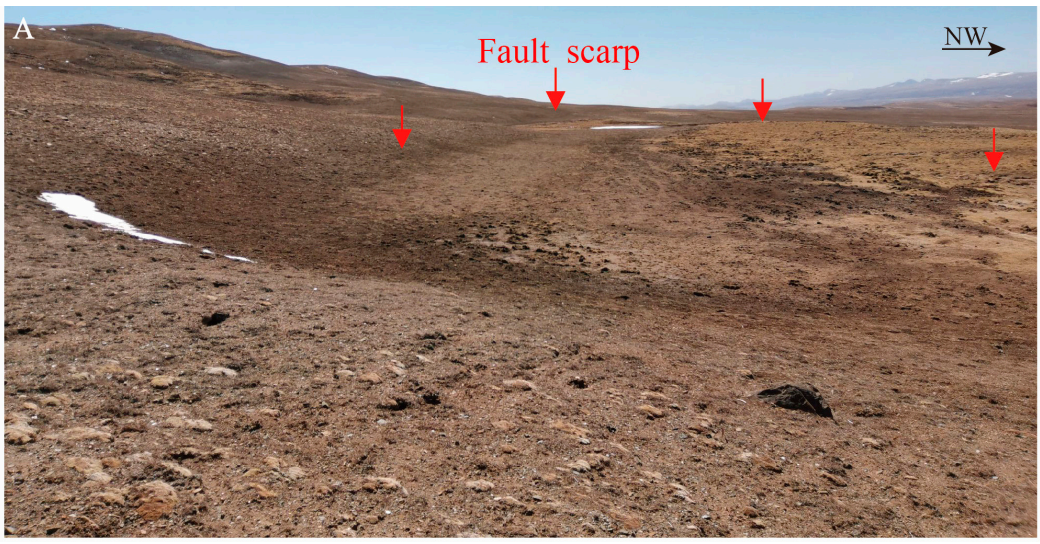

Figure 7. *Cont.*

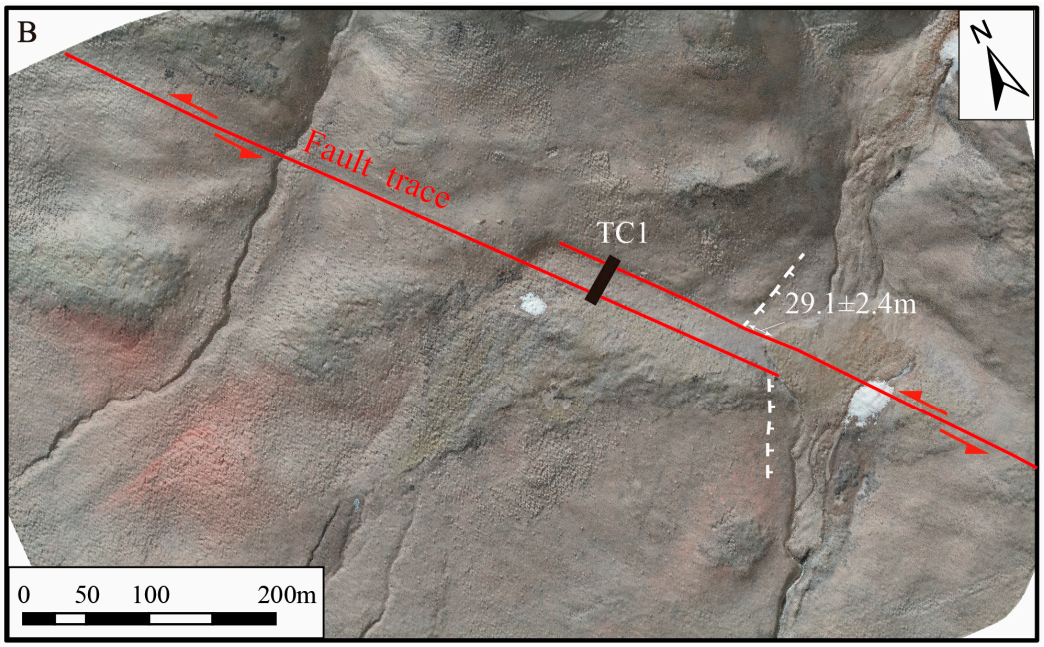

Figure 7. (**A**) Fault scarp and trough on the alluvial fan. (**B**) Fault trace and geomorphological characteristics around the location of trench TC1. Black rectangle identifies the location of trench TC1. The image was obtained using UAV photogrammetry. Red arrows mark the fault traces.

Near Jiatongma, the fault cuts across the piedmont diluvial fans, and a gully developed on the fan is left-laterally displaced by the fault (Figure 8A). The edge of the fan was displaced left-laterally by 10.4 m (Figure 8C). We excavated a geological section to collect ^{14}C samples (the black triangle in Figure 8A shows the sample position). The excavated profile revealed two sedimentary units (Figure 8B): unit U1, composed of brown sandy soil with some gravels; and unit U2, consisting of brown sandy gravel of diluvial origin. We collected a sample for ^{14}C dating (WC2022C-1), and the age was constrained to 3265–3106 cal BP. Therefore, we estimated the horizontal slip rate of the fault at 3.2 mm/a near Jiatongma. Horizontal slip rates of the WC fault, determined from the three sites, were 2.6, 2.0, and 3.2 mm/a; therefore, the mean slip rate and its standard deviation were estimated at 2.6 $\pm$ 0.6 mm/a.

4.2. Paleoseismological Investigation

(1) TC1 site

The TC1 site is to the east of the mouth of the Haqugama River, where the fault cut through the late Quaternary alluvial fan and produced a linear scarp and trough (Figure 7). There might be continuous sedimentary strata in the fault trough. Therefore, trench TC1 was excavated across the fault scarp and trough (Figure 7), and it revealed six stratigraphic units, details of which are elaborated in Table 2. From trench TC1, two paleoearthquake events were identified. On the basis of the sedimentation and deformation of the strata, the evidence for Event I is that faults F1 and F3 faulted units U1 and U2, and formed two colluvial wedges (W1 and W2) (Figure 9). According to radiocarbon dating results for samples WCTC-C14-01, WCTC-C14-04, and WCTC-C14-06 collected from units U2 and U4, Event I was constrained to between 15,052–14,782, and 5052–4862 cal BP. Because unit U4-2 is a sag pond deposit facies and represents a very low-energy depositional environment, it might have been caused by Event I, which means that the occurrence time of the event should be close to 5052–4862 cal BP. The evidence for Event II is that faults F1 and F2 faulted all the units. Constrained by the results of samples WCTC-C14-08 from U4-2 and WCTC-C14-12 from U5, Event II should have occurred after 673–628 cal BP.

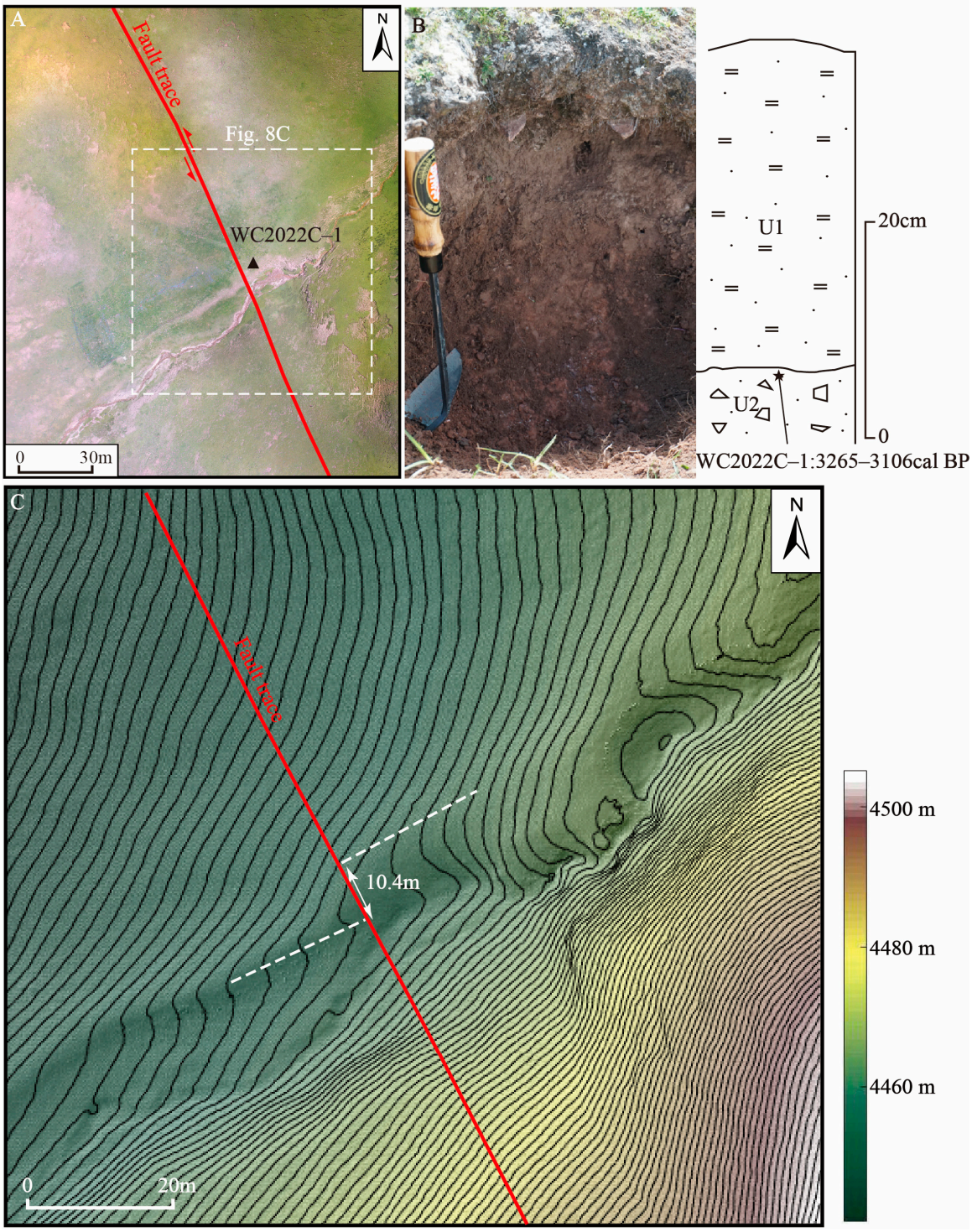

Figure 8. (**A**) Fault trace obtained using UAV photogrammetry. (**B**) Geological section for collecting dating samples and sample results from position of black triangle in (**A**). (**C**) The edge of the alluvial fan was left-laterally dislocated by 10.4 m, which was determined using LaDiCaoz_V2. It is shown within the white dotted rectangle in (**A**). The white dotted line shows the displaced edge of the alluvial fan in (**C**).

Table 2. Description of strata in trench TC1.

Unit No.	Description
U1	A yellow–brown gravel layer, and the gravel has an angular shape. The unit represents a diluvial deposit facies.
U2	A variegated sandy gravel layer (U2-1), partly deposited as lens-shaped sand layers (U2-2). The unit also represents a diluvial deposit facies.
U3	A khaki gravel layer, which is exposed only on the northeast side of the trench and pinches out toward the southwest.
U4	Divided into two subunits (Figure 9): unit U4-1 is a brick red, lens-shaped sand layer, and unit U4-2 is composed of sandy soil layers with some small gravels. The unit is a sag pond deposit facies.
U5	A dark-brown soil layer with many organic materials.

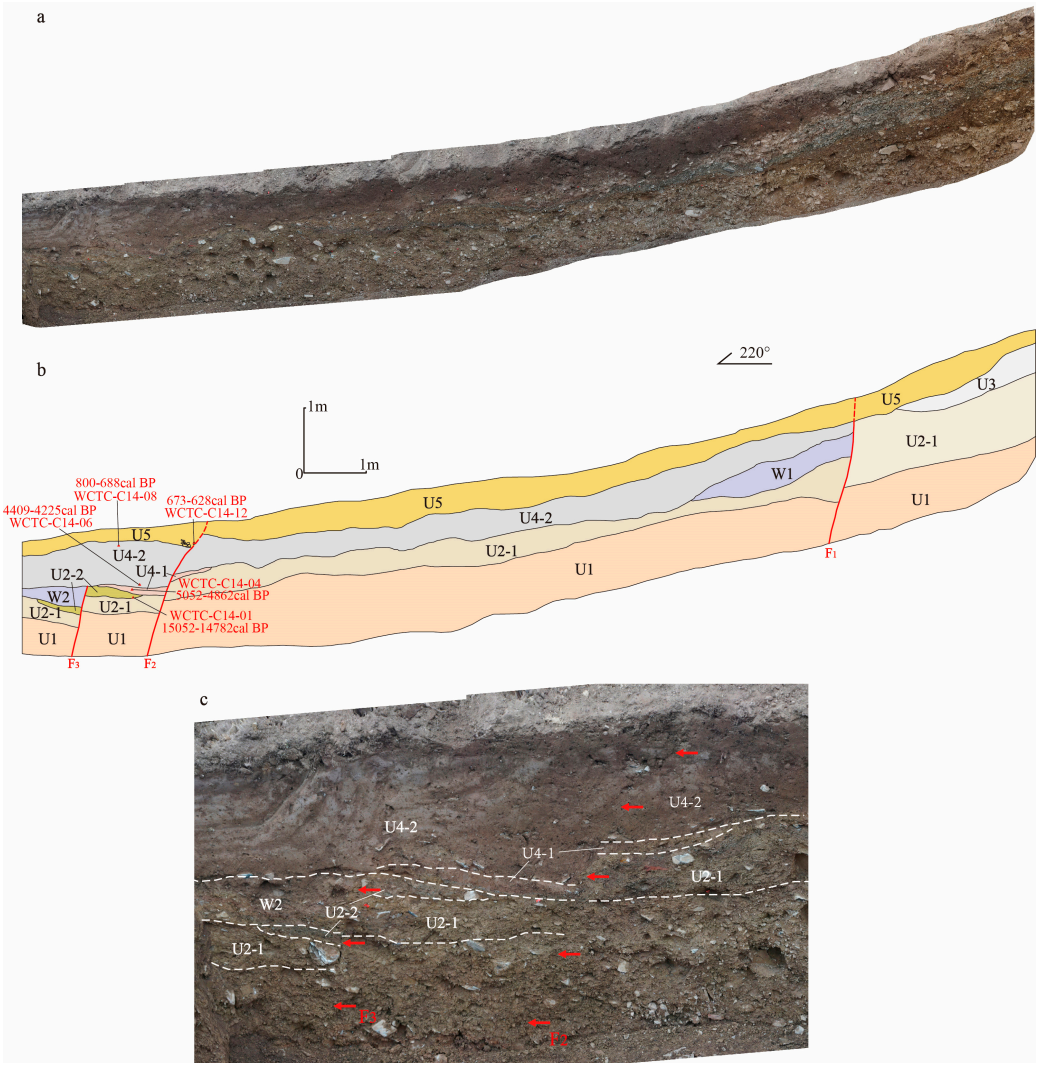

Figure 9. Photograph and geological interpretation of the section of TC1 in the position shown in Figure 7B. Red triangles are the sampling positions in the geological section. (**a**,**b**) are the trench photograph and interpretation profile, respectively. (**c**) shows the details of the faults and stratum. Red arrows mark the fault traces in (**c**).

(2) TC2 and TC3 site

The site of TC2 and TC3 is located on the alluvial fan in front of the mountain between the Haqugama and Erburong rivers (Figure 2). The fault formed a linear main scarp on the alluvial fan and some intermittently distributed secondary fault scarps (Figure 10). We excavated two trenches across the main scarp and identified eight units, the details of which are summarized in Table 3.

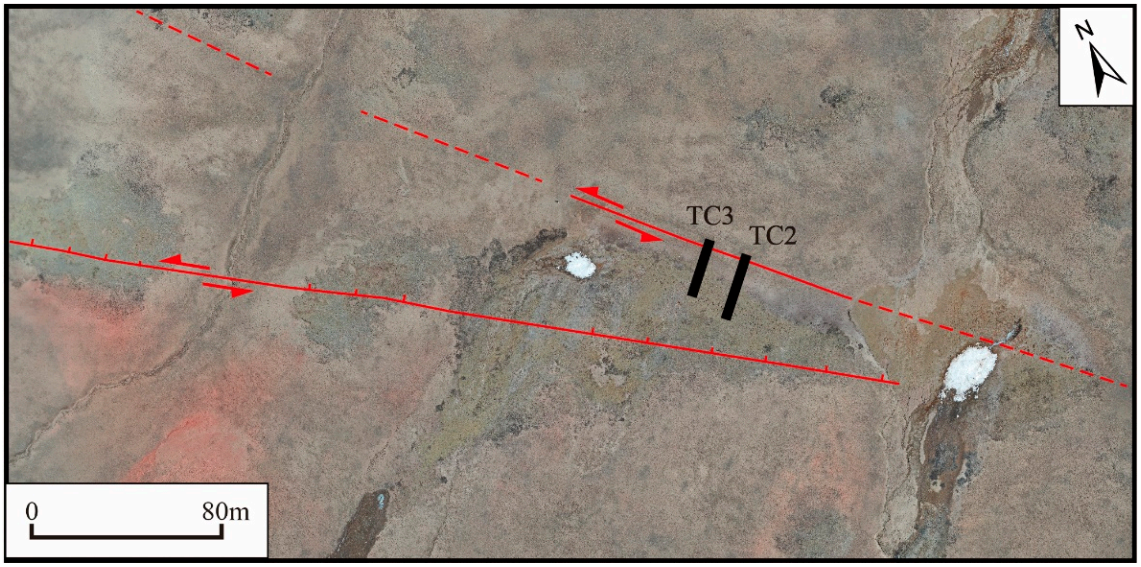

Figure 10. Fault trace and geomorphological characteristics around the site of trenches TC2 and TC3 obtained using UAV photogrammetry. Black rectangles identify the locations of trenches TC2 and TC3. The red dotted lines show the inferred fault traces.

Table 3. Description of the strata of trenches TC2 and TC3.

Unit No.	Description
U1	Deposited gravel that came from shallow metamorphic slate.
U2	A dark-gray sand layer with small amounts of gravel.
U3	A brick-red, lens-shaped sand layer.
U4	A yellow sandy gravel layer.
U5	A yellow sandy gravel layer with some interlayered gray sandy gravel.
U6	Gray sandy gravel layers and gravel layers deposited rhythmically.
U7	A variegated deposition of mixed sand and gravel, exposed only in trench TC2.
U8	A yellow–brown sandy soil layer.

Four earthquake events were identified following examination of trenches TC2 and TC1. In Event I, units U2–U4 were displaced by faulting that caused the units to bend and deform (Figures 11 and 12). In accordance with the carbon dating results for samples WCTC-02, WCTC-06, and WCTC-05 collected from units U2, U4, and U5, respectively, Event I was constrained to between 42,378–41,631 and 33,935–32,975 cal BP. The evidence for Event II revealed in the trenches is relatively weak, i.e., it can be identified only from the displacement of unit U5 by fault F2, and it was covered by the subsequent deposition of unit U6. In combination with the stratigraphic dating results (carbon dating samples WCTC-05, WCTC-11, and WCTC-12) from trenches TC2 and TC3, Event II was constrained to between 33,935–32,975 and 20,979–20,663 cal BP. The obvious evidence for Event III is that units U6 and U7 were displaced by the fault, and that the thickness of unit U8 that was deposited subsequently increased (Figures 11 and 13). The age of samples WCTC-11

and WCTC-14 is 20,517–20,258 and 2598–2496 cal BP, respectively (Figure 13). Thus, this event can be constrained to between 2598–2496 and 20,517–20,258 cal BP. In contrast to the carbon dating results of samples WCTC-11 and WCTC-14, the depositional age of unit U6 is much older than that of unit U8. The increase in the depositional thickness of unit U8 in the hanging wall of the fault is related to Event III. Therefore, the age of Event III is likely to be closer to 2598–2496 cal BP. The evidence for the latest event (Event IV) is that all of the units were faulted after 2598–2496 cal BP.

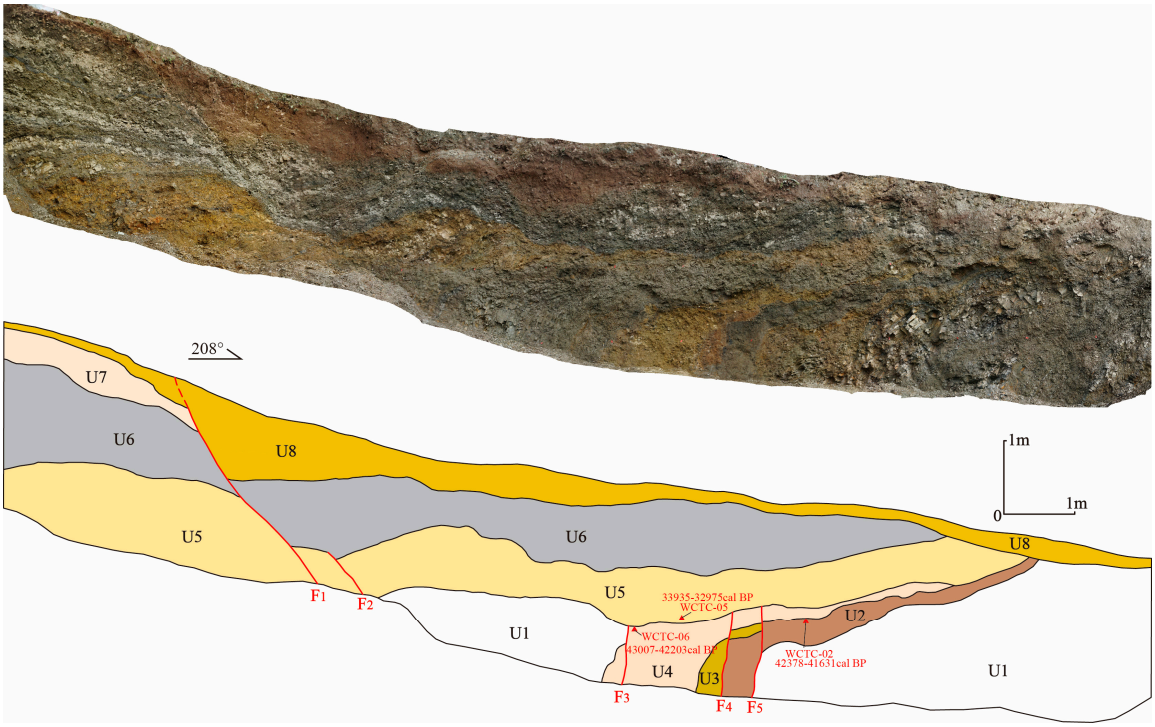

Figure 11. Photograph and geological interpretation of the section of TC2 in the position shown in Figure 10. Red triangles are the sampling positions in the geological section.

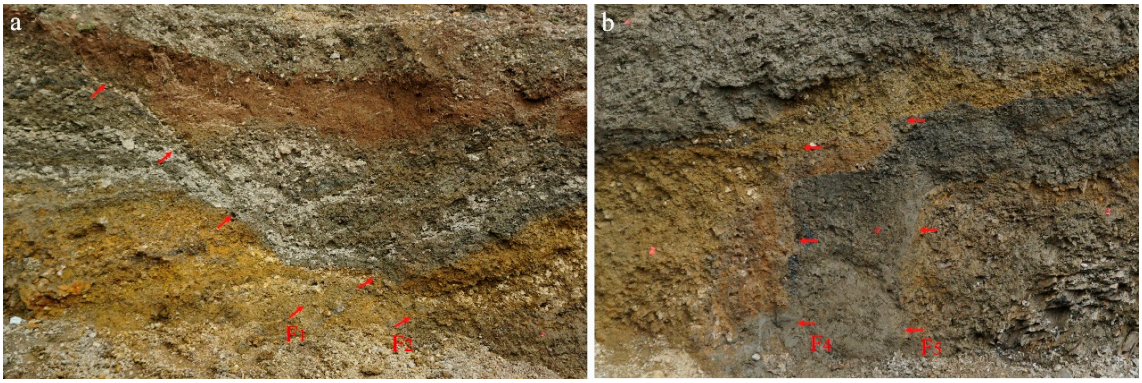

Figure 12. Photographs show the detail of the faults and stratum. Their positions are marked by the blue-dotted rectangle in Figure 11. Red arrows indicate the fault traces. (**a**) shows the details of the faults F1 and F2 in Figure 11. (**b**) shows the details of the faults F4 and F5 in Figure 11. Red arrows mark the fault traces.

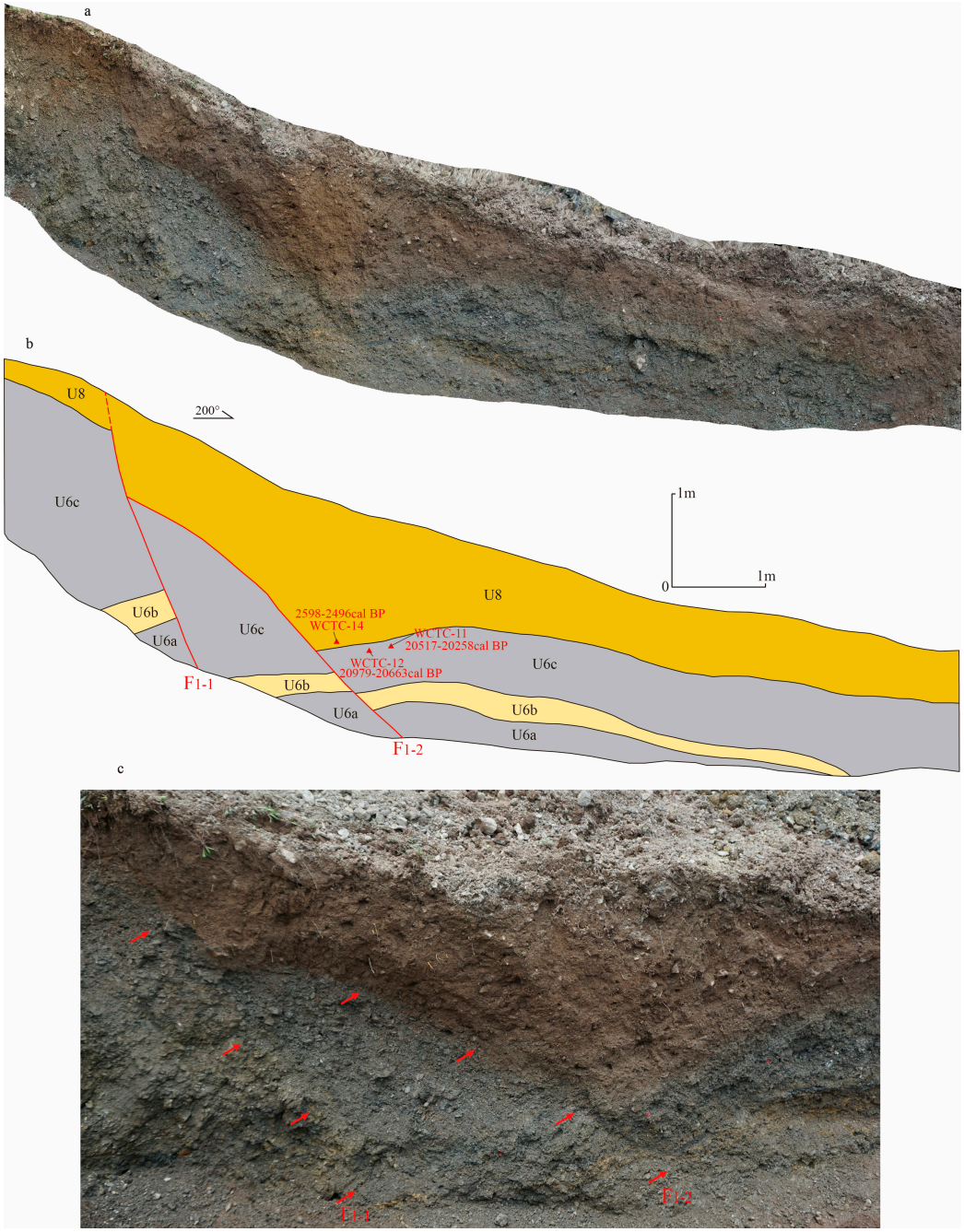

Figure 13. (**a**–**c**)Photograph and geological interpretation of the section of TC3 in the position shown in Figure 10. Red triangles are the sampling positions in the geological section. Red arrows show the fault traces. (**c**) shows the details of the fault traces, and red arrows mark the fault traces.

5. Discussion

The horizontal slip rate of the WC fault was estimated at 2.6 ± 0.6 mm/a during Holocene. Four paleoearthquake events and times of occurrence were determined in our study. These quantitative parameters of the WC fault were reported for the first time in this paper. In addition to the WC fault, there are other similar faults within the Bayan Har block, e.g., the AWC, MG, and DR faults, and the Holocene horizontal slip rate of each is approximately equivalent to that of the WC fault [8,9,11,40,41]. Furthermore, GPS velocity field data show that the slip rates of these faults have no obvious gradient of change [42], indicating that tectonic deformation within the block is continuous and diffuse. However, our study did not obtain the slip rate of the WC fault on larger time scales.

The characteristics and changes of the late Quaternary fault activity are an open question. Therefore, we need to constrain the late Quaternary fault activity and behavior of the WC fault, which allows for discussion on the characteristics of kinematics and dynamics in the entire Bayan Har Block.

The characteristics of the strata and the radiocarbon dating results of trenches TC1–TC3 indicate that four earthquake events occurred in the middle segment of the WC fault. The occurrence times of Events I and II are 42,378–32,975 and 33,935–20,663 cal BP, respectively. Event III was constrained to approximately 5052–4862 cal BP in trench TC1, but up to before 2598–2496 cal BP in trench TC2. In addition, the underlying strata (units U1 and U2 in TC1, and unit U6 in TC2 and TC3) before Event III are the same diluvial gravel layers. Moreover, the deposition of subsequent strata was affected by Event III. Therefore, we suggest that it is the same event which is recorded in the three different trenches. The sag pond deposit facies in trench TC1 represent a very low-energy and continuous depositional environment after Event III. Therefore, the reasonable time of Event III should be 5052–4862 cal BP. The latest event (Event IV) may occur after 673–628 cal BP, which is constrained by the evidence from trench TC1. In Event IV, all strata were displaced, and there are new small fault scarps on the surface along the fault that were caused by the earthquake. Furthermore, the times of the four events were constrained to 42,378–32,975, 33,935–20,663, 5052–4862, and after 673–628 cal BP by the characteristics of strata and radiocarbon data. In this earthquake sequence, the radiocarbon dating of the strata before Event III shows an older age than the strata after the event. The results indicate that: (1) the WC fault may represent a long quiet period of the major earthquake activity; (2) the strata present before Event III underwent a long time of denudation. However, we need to obtain more major earthquake sequences of other faults within the Bayan Har Block to understand the characteristics of major earthquake activity, and to discuss the mechanism of deformation of the block. The results of the earthquake sequence of the WC fault suggests that the recurrence interval of earthquake activity is as long as several thousand years. The latest earthquake was approximately 600 years ago. Therefore, the potential risk of a major earthquake on the middle segment of the WC fault is limited. The recurrence interval of major earthquakes on the WC fault is much larger than that of the boundary faults of the Bayan Har Block and the slip rate is also much smaller.

6. Conclusions

The middle segment of the WC fault has undergone Holocene activity with a left-lateral strike-slip rate of 2.6 ± 0.6 mm/a. This slip rate, which is approximately equivalent to that of other large NW-trending strike-slip faults within the Bayan Har Block, indicates that tectonic deformation inside the block is continuous. We identified four earthquake events dated to 42,378–32,975, 33,935–20,663, 5052–4862, and after 673–628 cal BP.

Author Contributions: Conceptualization, Investigation, Writing, review and editing, M.L.; Investigation, Y.D.; Investigation, Y.Q.; Investigation, C.L.; Writing, editing, W.W.; Field survey, H.Z. (Huiping Zhang) and H.Z. (Hong Zuo); Material and data collection, W.Z.; Investigation, C.X.; Material and data collection, L.Y., Y.G. and T.L. All authors have read and agreed to the published version of the manuscript.

Funding: This work was jointly funded by the State Key Laboratory of Earthquake Dynamics, Institute of Geology, CEA (LED2020B02), National Key Research and Development Program of China (2021YFC3000601), Special Fund of the Institute of Earthquake Forecasting, China Earthquake Administration (CEAIEF2022050502), Lhasa National Geophysical Observation and Research Station (NORSLS21-04) and the research team of earthquake sequence tracing and post-earthquake trend, China Earthquake Administration.

Data Availability Statement: The 12.5-m-resolution Shuttle Radar Topography Mission data are freely available from NASA (https://search.asf.alaska.edu/#/, accessed on 16 March 2023).

Acknowledgments: The seismic data in Figure 1 were provided by the Sichuan Earthquake Agency, Chengdu, China.

Conflicts of Interest: The authors declare no conflict of interest.

References

1. Pan, J.W.; Bai, M.K.; Li, C.; Liu, C.F.; Li, H.B.; Liu, D.L.; Marie-Luce, C.; Wu, K.Z.; Wang, P.; Lu, H.J.; et al. Coseismic surface rupture and seismogenic structure of the 2021-05-22 Maduo (Qinghai) MS7.4 earthquake. *Acta Geol. Sin.* **2021**, *95*, 1655–1670.
2. Gai, H.L.; Yao, H.S.; Yang, L.P.; Kang, T.B.; Ying, X.; Cheng, T.; Li, X. Characteristics and causes of coseismic surface rupture triggered by the"5. 22"MS7. 4 Earthquake in Maduo, Qinghai, and their significance. *J. Geomech.* **2021**, *27*, 899–912.
3. Tapponnier, P.; Peltzer, G.; Le Dain, A.Y.; Cobbold, P. Propagating Extrusion Tectonics in Asia: New Insights from Simple Experiments with Plasticine. *Geology* **1982**, *10*, 611. [CrossRef]
4. Zhang, P.-Z.; Shen, Z.; Wang, M.; Gan, W.; Burgmann, R.; Molnar, P.; Wang, Q.; Niu, Z.; Sun, J.; Wu, J.; et al. Continuous deformation of the Tibetan Plateau from global positioning system data. *Geology* **2004**, *32*, 809. [CrossRef]
5. Burchfiel, B.; Royden, L.; Van Der Hilst, R.; Hager, B.; Chen, Z.; King, R.; Li, C.; Lu, J.; Yao, H.; Kirby, E. A geological and geophysical context for the Wenchuan earthquake of 12 May 2008, Sichuan, People's Republic of China. *GSA Today* **2008**, *18*, 4. [CrossRef]
6. Xu, X.; Keller, G.R.; Gao, R.; Guo, X.; Zhu, X. Uplift of the Longmen Shan area in the eastern Tibetan Plateau: An integrated geophysical and geodynamic analysis. *Int. Geol. Rev.* **2015**, *58*, 14–31. [CrossRef]
7. Wen, X.Z. The 2008 Wenchuan, 2013 Lushan and 2017 Jiuzhaigou Earthquakes, Sichuan, in the last more than one Thousand Years of Rupture History of the Eastern Margin of the Bayan Har Block. *Acta Seismol. Sin.* **2018**, *40*, 255–267.
8. Liang, M.J.; Zhou, R.J.; Yan, L.; ZHAO, G.H.; Guo, H.M. The Relationships Between Neotectonic Activity of The Middle Segment of Dari Fault and Its Geomorphological Response, Qinghai Province, China. *Seismol. Geol.* **2014**, *36*, 28–38.
9. Liang, M.J.; Yang, Y.; Du, F.; Gong, Y.; Sun, W.; Zhao, M.; He, Q. Late Quaternary Activity of The Central Segment of The Dari Fault and Restudy of The Surface Rupture Zone of the 1947 M73/4 Dari Earthquake, Qinghai Province. *Seismol. Geol.* **2020**, *42*, 703–714.
10. Xiong, R.W.; Reng, J.W.; Zhang, J.L.; Yang, P.X.; Li, Z.M.; Hu, C.Z.; Cheng, C.Y. Late Quaternary Active Characteristics of the Gande Segment in the Maduo-Gande Fault Zone. *Earthquake* **2010**, *30*, 65–73.
11. Li, C.X.; Yan, D.Y.; Yang, H.; Xu, X.W. The Tectonic Activity Characteristics of Awancang Fault in the Late Quaternary, the Sub-strand of the Eastern Kunlun fault. *Seismol. Geol.* **2016**, *38*, 44–64.
12. Zhang, Y.M.; Li, M.F.; Meng, Y.Q. Research on Fault Activities and Their Seismogeological Implication in Bayan Har Mountain Area. *Res. Act. Fault* **1996**, *5*, 154–171.
13. Deng, Q.D.; Ran, Y.K.; Yang, X.P. *Distribution Map of Active Faults in China (1:4,000,000)*; Seismological Press: Beijing, China, 2007. (In Chinese)
14. Xu, X.W.; Han, Z.J.; Yang, X.P.; Zhang, S.M.; Yu, G.H.; Zhou, B.G.; Li, F.; Ma, B.Q.; Chen, G.H.; Ran, Y.K. *Seismotectonic Map in China and Its Adjacent Regions*; Seismological Press: Beijing, China, 2016. (In Chinese)
15. Wu, Z.H.; Zhou, C.J. *Distribution Map of Active Faults in China and Its Adjacent Sea Area (1:5,000,000)*; Geological Publishing House: Beijing, China, 2017. (In Chinese)
16. Liu, J.; Cheng, T.; Zhang, P.Z.; Zheng, W.J. Illuminating the active Haiyuan Fault, China by airborne light detection and ranging. *Chin. Sci. Bull.* **2013**, *58*, 41–45.
17. Zielke, O.; Arrowsmith, J.R.; Ludwig, L.G.; Akçiz, S.O. Slip in the 1857 and Earlier Large Earthquakes Along the Carrizo Plain, San Andreas Fault. *Science* **2010**, *327*, 1119–1122. [CrossRef]
18. Klinger, Y.; Etchebes, M.; Tapponnier, P.; Narteau, C. Characteristic slip for five great earthquakes along the Fuyun fault in China. *Nat. Geosci.* **2011**, *4*, 389–392. [CrossRef]
19. Zielke, O.; Klinger, Y.; Arrowsmith, J.R. Fault slip and earthquake recurrence along strike-slip faulits-contributions of high-resolution geomorphic data. *Tectophysics* **2015**, *638*, 43–62. [CrossRef]
20. Ren, Z.; Zhang, Z.; Chen, T.; Yan, S.; Yin, J.; Zhang, P.; Zheng, W.; Zhang, H.; Li, C. Clustering of offsets on the Haiyuan fault and their relationship to paleoearthquakes. *Geol. Soc. Am. Bull.* **2015**, *128*, 3–18. [CrossRef]
21. Liu, J.R.; Ren, Z.K.; Zhang, H.P.; Li, C.Y.; Zhang, Z.Q.; Zheng, W.J.; Li, X.M.; Liu, C.C. Late Quaternary slip rate of the Laohushan fault within the Haiyuan fault zone and its tectonic implications. *Chin. J. Geophys.* **2018**, *61*, 1281–1297.
22. Hudnut, K.W.; Borsa, A.; Glennie, C.; Minster, J.B. High-resolution topography along surface rupture of the 16 October 1999 Hector Mine, California, Earthquake (Mw 7.1) from airborne laser swath mapping. *Bull. Seismol. Soc. Am.* **2002**, *92*, 1570–1576. [CrossRef]
23. Oskin, M.E.; Arrowsmith, J.R.; Corona, A.H.; Elliott, A.J.; Fletcher, J.M.; Fielding, E.J.; Gold, P.O.; Garcia, J.J.; Hudnut, K.W.; Liu, J.; et al. Near-field deformation from the EI Mayor-Cucapah earthquake revealed by differential LIDAR. *Science* **2012**, *335*, 702–705. [CrossRef]
24. Zielke, O.; Arrowsmith, J.R. LaDiCaoz and LiDAR imager-MATLAB GUIs for LiDAR data handling and lateral displacement measurement. *Geosphere* **2012**, *8*, 206–221. [CrossRef]
25. Bemis, S.P.; Micklethwaite, S.; Turner, D.C.; James, M.R.D.; Akciz, S.E.; Thiele, S.T.; Bangash, H.A. Ground-based and UAV-Based photogrammetry: A multi-scale, high-resolution mapping tool for structural geology and paleoseismology. *J. Struct. Geol.* **2014**, *69*, 163–178. [CrossRef]

26. Angster, S.; Wesnousky, S.; Huang, W.; Kent, G.; Nakata, T.; Goto, H. Application of UAV Photography to Refining the Slip Rate on the Pyramid Lake Fault Zone, Nevada. *Bull. Seism. Soc. Am.* **2016**, *106*, 785–798. [CrossRef]
27. Enkelmann, E.; Weislogel, A.; Ratschbacher, L.; Eide, E.; Renno, A.; Wooden, J. How was the Triassic Songpan-Ganzi basin filled? A provenance study. *Tectonics* **2007**, *26*, 4007. [CrossRef]
28. Zhang, K.X.; Wang, G.C.; Cheng, F.N.; Xu, Y.D.; Luo, M.S.; Guan, X.H.; Zhao, L.S. Coupling bet ween the Uplift of Qinghai-Tibet Plateau and Distribution of Basins of Paleogene -Neogene. *Earth Sci.* **2007**, *32*, 583–597.
29. Chen, S.J.; Li, R.S.; Ji, W.H.; Zhao, Z.M.; Li, G.D.; Liu, R.L.; Dai, C.G.; Zhu, Y.T. Lithostratigraphy Character and Tectonic-Evolvement of Permian-Trias in the Bayankala Tectonic Belt. *Earth Sci.* **2011**, *36*, 393–408.
30. Ding, L.; Yang, D.; Cai, F.L.; Pullen, A.; Kapp, P.; Gehrels, G.E.; Zhang, L.Y.; Zhang, Q.H.; Lai, Q.Z.; Yue, Y.H.; et al. Provenance analysis of the Mesozoic Hoh-Xil-Songpan-Ganzi turbidites in northern Tibet: Implications for the tectonic evolution of the eastern Paleo-Tethys Ocean. *Tectonics* **2013**, *32*, 34–48. [CrossRef]
31. Roger, F.; Jolivet, M.; Malavieille, J. The tectonic evolution of the Songpan-Garzê (North Tibet) and adjacent areas from Proterozoic to Present: A synthesis. *J. Asian Earth Sci.* **2010**, *39*, 254–269. [CrossRef]
32. Song, B.W.; Zhang, K.X.; Xu, Y.D.; Hou, Y.F.; Ji, J.L.; Luo, M.S. Paleogene Tectonic-Stratigraphic Realms and Sedimentary Sequence in China. *Earth Sci.* **2020**, *45*, 4352–4369.
33. Shen, Z.-K.; Lü, J.; Wang, M.; Burgmann, R. Contemporary crustal deformation around the southeast borderland of the Tibetan Plateau. *J. Geophys. Res. Solid Earth* **2005**, *110*, B11409. [CrossRef]
34. Xu, X.W.; Weng, X.Z.; Cheng, G.H.; Yu, G.H. Discovery of the Longriba Fault Zone in Eastern Bayan Har Block, China and Its Tectonic Implication. *Sci. China Ser. D Earth Sci.* **2008**, *38*, 529–542. [CrossRef]
35. Ren, J.; Xu, X.; Yeats, R.S.; Zhang, S. Latest Quaternary paleoseismology and slip rates of the Longriba fault zone, eastern Tibet: Implications for fault behavior and strain partitioning. *Tectonics* **2013**, *32*, 216–238. [CrossRef]
36. Chen, C.Y.; Ren, W.G.; Meng, G.J.; Yang, P.X.; Hu, C.Z.; Su, X.N.; Su, J.F. Division, deformation and tectonic implication of active blocksin the eastern segment of Bayan Harblock. *Chin. J. Geophys.* **2013**, *56*, 4125–4141.
37. Johnson, K.; Nissen, E.; Saripalli, S.; Arrowsmith, J.R.; Mcgarey, P.; Scharer, K.; Williams, P.; Blisniuk, K. Rapid mapping of ultrafine fault zone topography with structure from motion. *Geosphere* **2014**, *10*, 969–986. [CrossRef]
38. Bi, H.Y.; Zheng, W.J.; Zeng, J.Y.; Yu, J.X.; Ren, Z.K. Application of SfM photogrammetry method to the quantitative study of active tectonics. *Seismol. Geol.* **2017**, *39*, 656–674.
39. Sun, W.; He, H.L.; Wei, Z.Y.; Gao, W.; Sun, H.Y.; Zou, J.J. Interpretation and analysis of the fine fault geometry based on high-resolution DEM data derived from UAV photogrammetric technique: A case study of Tangjiapo site on the Haiyuan fault. *Seismol. Geol.* **2019**, *41*, 1350–1365.
40. Liang, M.; Wu, W.; Yang, Y.; Du, F.; Zhou, W.; Zuo, H.; Liao, C.; Liu, S.; Zhang, H. Late Quaternary fault activity and deformation mechanism in the eastern Tibet Plateau (Dari fault, Bayan Har Block). *Quat. Int.* **2022**, *656*, 26–36. [CrossRef]
41. Zhan, Y.; Liang, M.J.; Sun, X.Y.; Huang, F.P.; Zhao, L.Q.; Gong, Y.; Han, J.; Li, C.X.; Zhang, P.Z.; Zhang, H.P. Deep structure and seisogenic pattern of the 2021.5.22 Madoi (Qinghai) Ms7.4 earthquake. *Chin. J. Geophys.* **2021**, *64*, 2232–2252.
42. Wang, M.; Shen, Z.-K. Present-Day Crustal Deformation of Continental China Derived from GPS and Its Tectonic Implications. *J. Geophys. Res. Solid Earth* **2020**, *125*, e2019JB018774. [CrossRef]